# EXCITATION AND DAMPING OF SLOW MAGNETOSONIC STANDING WAVES IN A SOLAR CORONAL LOOP

**M. Selwa[(1)], K. Murawski[(1)], and S. K. Solanki[(2)]**

*[(1)]Institute of Physics, UMCS, ul. Radziszewskiego 10, 20-031 Lublin, Poland*
*[(2)]Max-Planck-Institut für Sonnensystemforschung, Max-Planck-Str. 2, 37191 Katlenburg-Lindau, Germany*

## ABSTRACT

We consider slow magnetosonic standing waves that are impulsively excited in a solar coronal loop. The one-dimensional numerical model we implement includes the effects of nonlinearity. We evaluate numerically excitation and damping times of a standing wave in hot coronal loops on the basis of a parametric study. The results of the numerical simulations reveal that initially launched impulses trigger mainly the first or second standing waves, depending on the spatial location of these pulses. A parametric study shows that in the short loops considered here these standing waves are for most loop and pulse parameter values excited in $3-6$ wave periods and they are strongly damped over a similar time-scale.

Key words: solar corona; coronal loops.

## 1. INTRODUCTION

Coronal loop oscillations have become a subject of considerable recent observational and theoretical interest. Impulsively generated, standing slow waves in hot ($T > 6$ MK) loops have been detected with SOHO/SUMER (Wang et al. 2003a). It is interesting that these standing waves are strongly attenuated while they cool down (Curdt et al. 2003). Observations with Yohkoh, SUMER SOHO/EIT and TRACE/EUV have revealed that these loop oscillations seem to be often triggered by micro- or sub-flares near a loop foot-point (Wang et al. 2003b). In such cases the trigger may be hot plasma flow injected into the loop from one foot-point.

Several attenuation mechanisms have been proposed: wave leakage into the chromosphere (Ofman 2002), lateral wave leakage due to curvature of loops (Roberts 2000), phase mixing (Nakariakov 1999, Ofman, Aschwanden 2002), resonant absorption (Ruderman, Roberts 2002), non-ideal MHD effects (Roberts 2000). In particular, Ofman and Wang (2002) have found that thermal conduction leads to rapid damping of slow standing waves, with a less significant contribution from compressive viscosity (Ofman et al. 2002a). Ofman et al. (2002b) have shown that a nonlinear steepening of slow waves leads to their enhanced dissipation. Nakariakov et al. (2000a) have found that dissipation and stratification are the main factors influencing the slow wave evolution. De Moortel et al. (2002a) have deduced that thermal conduction can be important.

In another study, Nakariakov et al. (2004) and Tsiklauri et al. (2004) have demonstrated that in a coronal loop an impulsive energy release excites efficiently the second spatial harmonic. The considered model included the effects of gravitational stratification, heat conduction, radiative losses, external heat input and Braginskii bulk viscosity.

Our work is aimed at studying the excitation mechanism of slow standing waves. We discuss impulsively generated waves which are described by fully nonlinear one-dimensional ideal MHD equations. As a consequence of the one-dimensional assumption the Alfvén and fast magnetosonic waves are removed from the physical system which contains the slow waves only.

## 2. A NUMERICAL MODEL

We consider the coronal loop to lie along the $x$-direction. Additionally we assume that the velocity $\mathbf{V} = [V, 0, 0]$, magnetic field $\mathbf{B} = [B, 0, 0]$, and the plasma quantities depend on time $t$ and coordinate $x$ only. As a consequence of these assumptions we adopt the one-dimensional ideal MHD equations.

### 2.1 The loop equilibrium

We consider the equilibrium at which pressure $p_0 = const.$ and plasma is at rest, $V_0 = 0$. We choose the equilibrium density profile $\varrho_0$ which varies with $x$ in a way that $\varrho_0$ attains large values at loop foot-points which are settled at $x = 0$ and $x = L$, where $L = 50 \cdot 10^8$ cm is the loop length which corresponds to a loop radius of $13 - 16$ Mm. The loop is relatively short because short loops are easier to simulate. In Sect. 3.1.4 we also consider loops with other lengths. The mass density profile $\varrho_0(x)$ is similar to the profile that is implemented by Ofman (2002), i.e. $\varrho_0(x) = \varrho_c \left\{ \frac{d}{2} \left[ \tanh\left(s\left(x - x_{tr}\right) \cdot \left(x - L + x_{tr}\right)\right) + 1\right] + 1 \right\}$. Here $d$ is the ratio of the photospheric mass density $\varrho_{ph}$ to the coronal mass density $\varrho_c = 10^{-15}$ g cm$^{-3}$. We allow this parameter to vary in the range $10^4 \leq d \leq 10^8$. The quantity $s = 0.5 \cdot 10^{-17}$ cm$^{-1}$ denotes the slope of $\varrho_0(x)$ at the loop foot-points, and $x_{tr} = 0.2842 \cdot 10^8$ cm corresponds to the position of the transition region. As $T_0(x) \sim p_0/\varrho_0(x)$, the plasma temperature $T_0$ is higher at the solar corona than at the foot-points. We also choose and hold fixed the sound speed in the solar corona $c_s = \sqrt{\gamma p_0/\varrho_0(x = L/2)} = 0.35 \cdot 10^8$ cm s$^{-1}$.

### 2.2 Perturbations

Consider a coronal loop that is described by the ideal one-dimensional MHD equations. Perturbations can be

excited in such a loop in numerous ways. Here we focus our attention on impulsively excited waves. We launch a hot pulse in the mass density, pressure and velocity. This pulse has the following form:

$$\delta\varrho(x,t=0) = A_\varrho \exp\left[(x-x_0)^2/w^2\right] , \quad (1)$$

$$\delta p(x,t=0) = A_p \exp\left[(x-x_0)^2/w^2\right] , \quad (2)$$

$$\delta V(x,t=0) = A_V \exp\left[(x-x_0)^2/w^2\right] , \quad (3)$$

where $A_\varrho$, $A_p$ and $A_V$ are initial amplitudes of the pulse, $x_0$ its initial position and $w$ its initial width.

## 3. NUMERICAL RESULTS

In this part of the paper we present numerically obtained results for various run parameters. The plasma equations are solved numerically with the FLASH code (Fryxell et al. 2000). For most numerical runs 300 blocks are chosen. Each block contains 8 grid cells. Free boundary conditions are used at the boundaries of the simulation region. All physical quantities are measured in cgs units.

We discuss first and second standing waves which are triggered by temperature perturbations and pay particular attention to excitation and damping times of these modes. Our simulations show that these lowest modes are the dominantly excited ones for the pulse parameters employed.

### 3.1 Excitation by temperature perturbation

We consider now the case of ideal plasma for which there is no velocity perturbation. In this case slow waves are excited solely by temperature perturbations which are given by Eqs. (1)-(3), with $A_\varrho = 0.125\,\varrho_0(x_0)$ and $A_p = 0.25\,p_0$ and $A_V = 0$. We launch the pulses of Eqs. (1)-(2) with a width of $w = L/40$, which is a typical value that is determined from observations (Nakariakov et al. 2004). We also carry out a parameter study in which parameters are allowed to vary around the adopted fiducial values. We consider first in some detail three cases which correspond to different positions of the initial pulses: (a) $x_0 = L/4$, (b) $x_0 = L/2$, (c) $x_0 = 0$.

#### 3.1.1 Pulses at a quarter of the loop length and at the apex of the loop

If the initial pulse $x_0 = L/4$ ($x_0 = L/2$) the first (second) standing wave is excited. Fig. 1 displays spatial profiles of these waves at given moments of time. As the first standing wave is twice as long as the second wave (Fig. 1), the first wave is less sensitive to the inhomogeneous medium and essentially it occupies the cavity over all its length $L$. The second standing wave is more sensitive to the inhomogeneity than the first wave, resulting in enhanced energy leakage into the photosphere.

Time-signatures of the perturbed mass density $\delta\varrho$ and velocity $V$ which are detected at the spatial point $x = L/4$ are shown in Fig. 2 for a time interval after the initial high frequency power has died away.

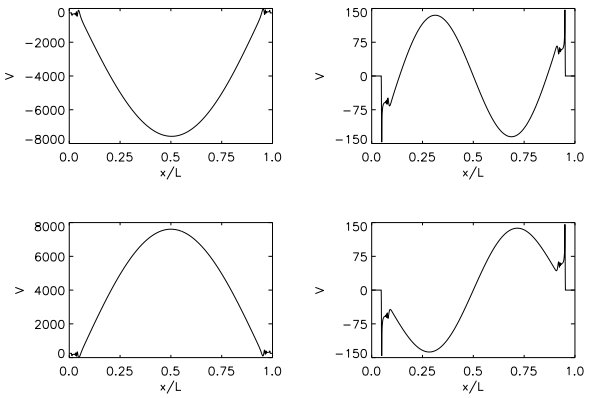


*Figure 1. Spatial profiles of the velocity $V(x, t = 18.842\ T_1)$ (left top panel), $V(x, t = 19.274\ T_1)$ (left bottom panel), $V(x, t = 37.841\ T_2)$ (right top panel), $V(x, t = 38.281\ T_2)$ (right bottom panel) for the mass density contrast $d = 10^8$, the pulse width $w = L/40$, the pulse position $x_0 = L/4$ (left panels), and $x_0 = L/2$ (right panels). Left (right) profiles correspond to the first (second) standing wave.*

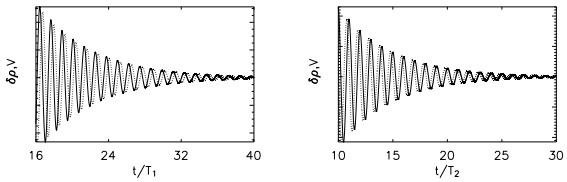


*Figure 2. Time-signatures of the perturbed mass density $\delta\varrho(x = L/4, t)$ (solid line) and velocity $V(x = L/4, t)$ (dashed line) for $d = 10^8$, $w = L/40$, $x_0 = L/4$ (left panel) and $x_0 = L/2$ (right panel).*

Oscillation amplitudes decrease with time as a consequence of wave damping due to energy leakage into the photosphere.

In all considered cases the presence of the standing wave in the system is evaluated on the basis of the normalized phase shift $\delta\phi$, for the first ($n = 1$) or second ($n = 2$) standing waves. We establish *an excitation criterion* according to which a standing wave is present in the system if $\delta\phi$ departs by 20% from $1/4$, since the quarter period lag is a signature of the analytical solution, *viz.*

$$\frac{1}{4}\cdot 80\% \le \delta\phi \le \frac{1}{4}\cdot 120\%. \quad (4)$$

This criterion is fulfilled for $t > t_{min}$. As the standing wave excitation time we assume $t_{min}$. According to this criterion the first (second) standing wave is excited at $t \approx 6\ T_1$ ($t \approx 3.5T_2$), where $T_1$ and $T_2$ are the analytically evaluated periods that are expressed by

$$T_n = \frac{2L_{eff}}{nc_s}. \quad (5)$$

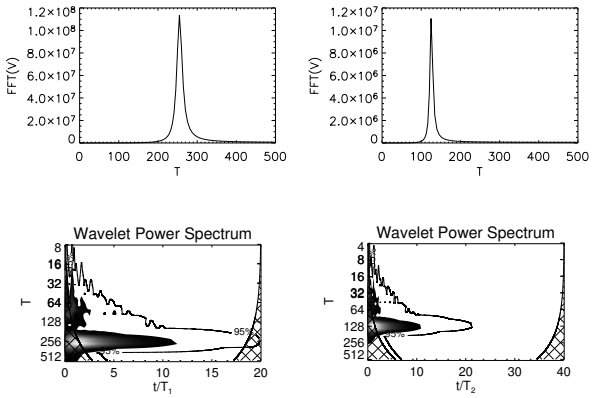


*Figure 3. Spectra of the velocity $V(x = L/4, t)$ of Fig. 2. The Fourier spectra are displayed in the top panels and the corresponding wavelet spectra are presented in the bottom panels. Note, that both the Fourier and wavelet analysis lead to the wave periods $T_1 \approx 254$ s, $T_2 \approx 125$ s, where $T_n$ is the $n$-th standing wave period. The hatched area in the lower frames indicates regions where the wavelet transform is less accurate.*

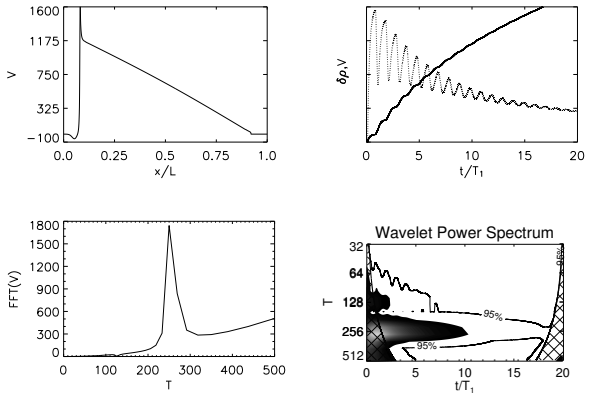


*Figure 4. A spatial velocity profile at $t \approx 20\ T_1$ (left top panel), time-signatures (right top panel) of the perturbed mass density $\delta\varrho(x = L/4, t)$ (solid line) and velocity $V(x = L/4, t)$ (dotted line) for $d = 10^8$, $w = L/40$ and $x_0 = 0$. The corresponding Fourier and wavelet power spectra are displayed in the bottom panels.*

Here $n$ denotes the standing wave number, $c_s$ is the sound speed, and $L_{eff}$ is the effective loop length. From Fig. 1 we estimate that $L_{eff} \approx 45 \cdot 10^8$ cm and then $T_1 \approx 257$ s and $T_2 \approx 128$ s. These values are close to the results of the fast Fourier transform (FFT) and wavelet analyses (Fig. 3). Small differences result from the fact that the effective length of the cavity is lower than $L$ and it differs for the case of $n = 1$ nad $n = 2$. Moreover, $c_s$ is an inhomogeneous function of $x$ in our simulations, but is assumed to be $x$-independent when evaluating Eq. (5).

We have restricted the Fourier analysis to $t > 3\ T_1$ in order to remove the transient signal at the initial stage of temporal evolution. This signal is discernible in the wavelet power spectrum (Fig. 3) which has been obtained using a Morlet mother function (Torrence and Compo 1998)

$$\psi(\eta) = \pi^{-1/4} e^{im\eta} e^{-\eta^2/2}$$

with $m = 6$. The wavelet transform was applied to the full time series. The solid contour represents $95\%$ confidence.

### 3.1.2 A pulse at a foot-point

We discuss now the case of the initial pulse of Eqs. (1)-(2). This pulse is launched at the loop foot-point located at $x = 0$. Fig. 4 displays the corresponding results. As a result of a hot initial pulse, plasma is heated locally at the loop foot-point. Just warmed up and dense photospheric plasma leaves the excitation region and fills up the coronal loop. As a consequence of that $\delta\varrho$ grows with time (top right panels). The mean flow is directed to the loop center and its efficiency declines both spatially in the region $x > x_0$ (left top panel) and with time (right top panel). Velocity power spectra (bottom panels) reveal the wave period of the first standing wave, $T_1$. The background in the Fourier power spectrum is introduced by the velocity drift. The wave excitation time $t_{\rm ex} \approx 3\ T_1$ and the damping time $\tau \approx 5\ T_1$. Qualitatively similar results have been obtained in the case of the initial pulse launched in the photosphere at $x_0 = -L/50$, i.e. outside the loop, corresponding to subsurface layers of the Sun (not shown) and recently by Tsiklauri et al. (2004) who have discussed the case of heat deposition at a loop-foot point.

### 3.1.3 Excitation of a packet of standing waves

Setting the initial pulses in different parts of the loop leads to the excitation of different waves.. In some cases we do not observe a single standing mode but a packet of modes in which the first and the second standing mode have the highest contribution. Fourier spectra show that an almost pure second standing wave is excited when the initial pulse is launched at the loop apex. Moving the excitation point from the loop apex to the foot-points results in an excitation of the first mode. For excitation points that are close to, but not exactly at $x_0 = L/2$ we observe that the Fourier power in the second standing mode is much higher than in the first standing mode, while for $x_0 = 3L/8$ the first mode dominates (Fig. 5). The third and higher modes are also initially present in the system. However, their Fourier power is much lower and they are damped more rapidly, so that we can distinguish them only by analysing the initial stage of the simulation time.

### 3.1.4 Parametric studies of wave excitation and damping times

In this part of the paper we present results of parametric studies. We vary several parameters such as the pulse position $x_0$, density contrast $d$, pulse width $w$, temperature

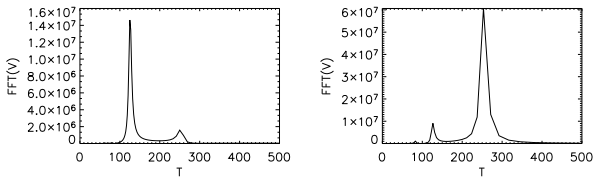


*Figure 5. Fourier spectra of the velocity $V(x = L/4, t)$ for $d = 10^8$, $w = L/40$ and $x_0 = 0.475L$ (left panel) and $x_0 = 0.375L$ (right panel). First (right panel) and second (left panel) standing modes dominate.*

of initial pulses, and perturbations in velocity $A_V$. We analyze how the standing wave excitation time $t_{ex}$ and damping time $\tau$ depend on these parameters.

We first filter out non-oscillatory components from the time-signatures $\varrho(x_0 = L/4, t)$ and $V(x_0 = L/4, t)$ to remove trends, such as seen in the upper right panel of Fig. 4, and to get a pure signal which corresponds solely to oscillations. The filtering is done by the code that was originally developed by Ofman (2002). We estimate the excitation time $t_{ex}$ using the criterion described by Eq. (4), while for the damping time $\tau$ we fit an envelope of a velocity profile into the following formula:

$$V(x = x_d, t) = V_0 \, \exp\left[-\frac{(t - t_{ex})}{\tau}\right], \, t \geq t_{min} \, ,$$

where $x_d$ denotes the detection point, $V_0$ is the amplitude of the velocity $V$ at time $t_{ex}$.

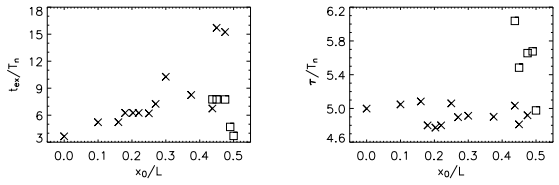


*Figure 6. The normalized standing wave excitation time $t_{ex}/T_n$ (left panel) and the normalized damping time $\tau/T_n$ (right panel) vs. the normalized pulse position $x_0/L$ for $d = 10^8$ and $w = L/40$. The crosses (squares) correspond to the first (second) standing waves.*

We first consider the dependence of $t_{ex}$ and $\tau$ on the location $x_0$ of the initial pulse. Fig. 6 shows that the first (second) standing wave excitation time $t_{ex}$ generally grows (declines) as the pulse position $x_0$ moves from the loop footpoint ($x_0 = 0$) to its apex ($x_0 = L/2$). In the case of the first standing wave, the damping time depends weakly on $x_0$, with a slight tendency to decrease with $x_0$ (right panel of Fig. 6). The second standing wave damping time decreases as $x_0$ approaches $L/2$.

These results support evidence that excitation and damping times are not constant but depend on the location of the initial pulse. Excitation time varies from its lowest value of 3 $T_1$ for $x_0 = 0$ to its highest value of 16 $T_1$ for $x_0 = 0.45$ $L$ for the first standing wave (and from 3 $T_2$ for $x_0 = L/2$ to 8 $T_2$ for $x_0 = 0.45$ $L$ in the case of the second standing wave). The obtained values of damping time are in the range $4.7\ T_1 < \tau < 5.2\ T_1$ for the first standing wave and $5\ T_2 < \tau < 6.1\ T_2$ for the second standing wave for which the lowest (highest) value is obtained for $x_0 = L/2$ (for $x_0 = 0.44\ L$). Note that $T_1 \approx 2T_2$, so that in absolute terms the 2nd wave is damped more rapidly than the first wave.

We conclude from the above results that the first (second) standing wave is excited most efficiently by an initial pulse that is located in the neighborhood of a loop foot-point (of the loop apex). At these points the excitation (damping) time of these waves is equal to 3 (5) periods, corresponding roughly to 13 min (11 min).

The standing wave excitation time varies with the density contrast $d$ (Fig. 7). For high values of $d$ the first standing wave is excited less efficiently than for low values, for which $t_{ex}$ attains its minimum; the excitation time is doubled as the density contrast is changed by four orders of magnitude. At the smallest (largest) considered value of $d = 10^2$ ($d = 10^8$) the damping time is 2.5 $T_1$ (6.2 $T_1$). From these results we draw the conclusion that the first standing wave is excited faster in low density contrast regions, as such a structure is more susceptible to energy leakage at the foot-points. As a consequence of that it is easier for a perturbation to adjust to standing waves profiles. Obviously, damping of the wave is enhanced and the damping time is of the order of a few wave periods. About twice weaker damping occurs at $d = 10^8$ than at $d = 10^2$, although the dependence of $\tau$ on $d$ is complex.

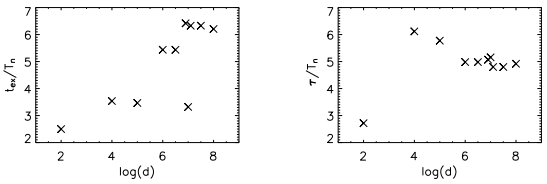


*Figure 7. The normalized first standing wave excitation time (left panel) and the normalized damping time (right panel) vs.* $\log d$ *for $w = L/40$ and $x_0 = L/4$.*

The standing wave excitation time depends on the pulse width $w$ (Fig. 8). For a sufficiently wide pulse the first standing wave is excited faster by wider pulses although there is significant scatter (left panel). The damping time oscillates around a value of about 4.8 $T_1$, within a relatively narrow range implying that it is almost independent of $w$. These results are a consequence of the fact that wider pulses are closer to the sine function of $x$ of the analytical standing wave spatial profile; sufficiently wide pulses adjust faster to the standing waves.

In the case of the second standing mode, its excitation

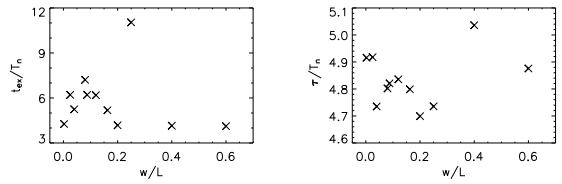


*Figure 8. The normalized first standing wave ($n = 1$) excitation time $t_{ex}/T_n$ (left panel) and the damping time $\tau/T_n$ (right panel) vs. the pulse width $w$ for $d = 10^8$ and $x_0 = L/4$.*

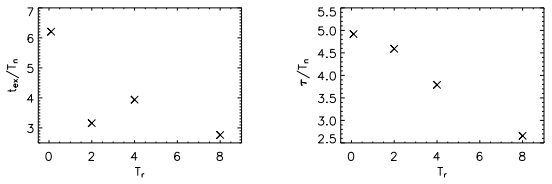


*Figure 9. The normalized first standing wave excitation time (left panel) and damping factor (right panel) vs. the normalized pulse temperature $T_r$ for $d = 10^8$, $w = L/40$ and $x_0 = L/4$.*

and damping times vary with the pulse width (Tab. 1). For a very wide pulse the second standing wave is excited slower than by narrower pulses, but its damping time is slightly shorter. Note, that even for $w = 3 \cdot 10^9$ cm, when the initial pulse is close to the sine function of $x$, corresponding to the shape of the first wave, it is the second, not the first mode which is excited for the pulse position $x_0 = L/2$.

*Table 1. The excitation time $t_{ex}$, and damping time $\tau$ for two different widths of the pulse in the case of the second ($n = 2$) standing wave for $d = 10^8$ and $x_0 = L/2$.*

| $w/L$ | $t_{ex}$ [s] | $\tau$ [s] |
|---|---|---|
| 0.025 | 463 | 603 |
| 0.6 | 1050 | 565 |

So far, we have discussed the initial pulses of constant relative temperature $T_r = T_p/T_c = 0.1$, where $T_p$ is the temperature of the initial pulse and $T_c$ is the temperature of the corona. This temperature is realized through the choice of the pulse amplitudes $A_\varrho = 0.125\varrho_0(x_0)$, $A_p = 0.25p_0$. It is worth quantifying the influence of $T_r$ on the mode excitation time $t_{ex}$ and the damping time $\tau$. To do so, we consider three values of the temperature ratio: $T_r = 2$ ($A_\varrho = 0.125\varrho_0(x_0)$, $A_p = 1.25p_0$), $T_r = 4$ ($A_\varrho = 0.125\varrho_0(x_0)$, $A_p = 3.5p_0$), $T_r = 8$ ($A_\varrho = 0.125\varrho_0(x_0)$, $A_p = 8.0p_0$). Fig. 9 summarizes results of the corresponding numerical experiments. A warmer pulse leads to more efficient standing wave excitation as the excitation time declines with $T_r$. The standing wave is more rapidly damped for higher values of $T_r$. Given that $T_r$ changes by a factor of 80, the induced changes in $t_{ex}$ and $\tau$ are relatively small (factor of 2).

We compare now four cases which correspond to the following loop lengths $L_0$: (a) $L_0 = L = 50 \cdot 10^8$ cm, (b) $L_0 = 2L$, (c) $L_0 = 3L$, and (d) $L_0 = 6L$. The pulse position was chosen as $x_0 = L_0/4$. The excitation time decreases with the loop length for narrow pulses (Fig. 10). The normalized damping time $\tau/\tau_n$ generally grows with the loop length $L_0$ (right panel). Note that since $T_n \sim L_0$ the results must be considered carefully. E.g. $t_{ex}$ actually grows somewhat with $L_0$ (in secs).

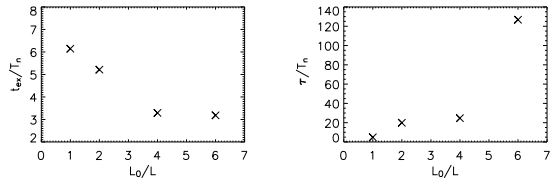


*Figure 10. The normalized first standing wave excitation time (left panel) and damping time (right panel) vs. the normalized loop length $L_0$, for $d = 10^8$, $x_0 = L_0/4$ and $w = L/40$. Note that $T_n$ now corresponds to the expected period for the appropriate loop length.*

### 3.2 Velocity pulses

We consider now a case that is similar to the cases discussed above. The only difference is that to the mass density and pressure perturbations we add a non-zero pulse in velocity. We choose and hold fixed $A_V = 0.125c_s(x_0)$. In the case of $x_0 = L/4$ the first standing wave is generated at $t_{ex} \approx 7\ T_1$ which is a little larger than in the case of $A_V = 0$ (Fig. 11). The damping time attains a value of $\tau \approx 5.5\ T_1$ which is $10\%$ higher than without the velocity pulse. From this result we conclude that the first mode is weakly affected by the presence or absence of velocity perturbations.

In the case of $x_0 = L/2$ and the second standing wave (squares) the excitation time is larger than in the case of $A_V = 0$ while the damping time becomes very slightly smaller than without the velocity pulse.

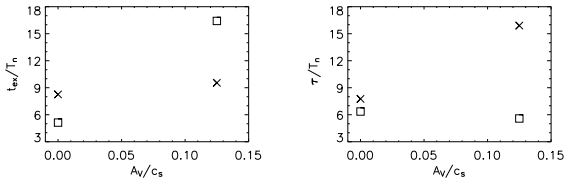


*Figure 11. The normalized first standing wave excitation time (left panel) and damping time (right panel) vs. the velocity amplitude of the initial pulse, $A_V$, for $d = 10^8$, $w = L/40$, $x_0 = L/4$ (crosses) and $x_0 = L/2$ (squares).*

## 4. SUMMARY

In this paper we have considered the excitation and damping of slow standing waves in a solar coronal loop that is approximated by a one-dimensional plasma. Our model implements nonlinearities and impulses in plasma quantities. A Fast Fourier transform and wavelet analysis of temporal wave profiles have shown that in a loop the first or second standing slow waves are excited depending on the location of the trigger. We have worked out a simple criterion for the presence of a standing wave. This criterion is based on a phase shift between the perturbed mass density $\delta\varrho$ and velocity $V$. The time which is required for a standing wave to be set up in a loop from a hot initial pulse is of the order of $3-6$ wave periods and it varies, depending on parameters of the plasma such as an initial location of the pulse, the density contrast or a pulse width. In the case of a wide and strong pulse as well as of heated plasma this time-scale is shorter.

## ACKNOWLEDGMENTS

The authors express their cordial thanks to Leon Ofman for providing his code for the evaluation of damping time. MS expresses her thanks to the conference organisers for their partial financial support. MS's & KM's work was financially supported by the grant from the State Committee for Scientific Research Republic of Poland, with KBN grant No. 2 PO3D 016 25. The FLASH code is provided by ASCI (Alliances Center for Astrophysical Thermonuclear Flashes) at the University of Chicago. Wavelet software is disseminated by C. Torrence and G. Compo, and is available at URL http://paos.colorado.edu/research/wavelets.

## REFERENCES

Aschwanden M., Fletcher L., Schrijver C., Alexander D., 1999, ApJ 520, 880

Curdt W., Wang T.J., Dammasch T.E., Solanki S.K., 2003, Hvar Obs. Bull. 27, 83

De Moortel I., Hood A.W., 2003, A&A 408, 755

De Moortel I., Hood A.W., Ireland J., 2002a, A&A 381, 311

De Moortel T., Hood A.W., Ireland J., Walsh R.W., 2002b, Solar Phys. 209, 89

Fryxell B., Olson K., Ricker P., et al., 2000, ApJS 131, 273

Nakariakov V.M., Ofman L., DeLuca E.E., et al., 1999, Science 285, 862

Nakariakov V.M., Verwichte E., Berghmans D., Robbrecht E., 2000, A&A 362, 1151

Nakariakov V.M., Tsiklauri D., Kelly A., et al., 2004, A&A 414, L25

Ofman L., 2002, ApJ 568, L135

Ofman L., Wang T.J., 2002, ApJ 580, L85

Ofman L., Aschwanden M., 2002, ApJ 576, L153

Ofman L., Nakariakov V. M., Sehgal N., 2000, ApJ 533, 1071

Roberts B., 2000, Solar Phys. 193, 139

Ruderman M.S., Roberts B., 2002, ApJ 577, 475

Torrence C., Compo G.P., 1998, Bull. Amer. Meteor. Soc. 79, 61

Tsiklauri D., Nakariakov V.M., Arber T.D., Aschwanden M.J., 2004, A&A 422, 351

Wang T.J., Solanki S.K., Curdt W., et al., 2002, ApJ 574, L101

Wang T.J., Solanki S.K., Innes D.E., et al., 2003a, A&A 402, L17

Wang T.J., Solanki S.K., Curdt W., et al., 2003b, A&A 406, 1105

Zingale M., Dursi L.J., ZuHone J., et al., 2002, ApJS 143, 539